Monthly Notices
of the
ROYAL ASTRONOMICAL SOCIETY

Mon. Not. R. Astron. Soc. (2011) doi:10.1111/j.1365-2966.2011.19784.x

High-precision transit observations of the exoplanet WASP-13b with the RISE instrument

S. C. C. Barros,[1⋆] D. L. Pollacco,[1] N. P. Gibson,[2] F. P. Keenan,[1] I. Skillen[3] and I. A. Steele[4]

[1]*Astrophysics Research Centre, School of Mathematics and Physics, Queen's University Belfast, University Road, Belfast BT7 1NN*
[2]*Department of Physics, University of Oxford, Denys Wilkinson Building, Keble Road, Oxford OX1 3RH*
[3]*Isaac Newton Group of Telescopes, Apartado de Correos 321, E-38700 Santa Cruz de la Palma, Tenerife, Spain*
[4]*Astrophysics Research Institute, Liverpool John Moores University, Wirral CH61 4UA*

Accepted 2011 September 6. Received 2011 August 23; in original form 2011 July 1

ABSTRACT

WASP-13b is a sub-Jupiter mass exoplanet orbiting a G1V type star with a period of 4.35 d. The current uncertainty in its impact parameter ($0 < b < 0.46$) results in poorly defined stellar and planetary radii. To better constrain the impact parameter, we have obtained high-precision transit observations with the rapid imager to search for exoplanets (RISE) instrument mounted on 2.0-m Liverpool Telescope. We present four new transits which are fitted with a Markov chain Monte Carlo routine to derive accurate system parameters. We found an orbital inclination of $85\overset{\circ}{.}2 \pm 0\overset{\circ}{.}3$ resulting in stellar and planetary radii of $1.56 \pm 0.04\,\mathrm{R}_{\odot}$ and $1.39 \pm 0.05 R_{\mathrm{Jup}}$, respectively. This suggests that the host star has evolved off the main sequence and is in the hydrogen-shell-burning phase. We also discuss how the limb darkening affects the derived system parameters. With a density of $0.17\rho_{\mathrm{J}}$, WASP-13b joins the group of low-density planets whose radii are too large to be explained by standard irradiation models. We derive a new ephemeris for the system, $T_0 = 245\,5575.5136 \pm 0.0016$ (HJD) and $P = 4.353\,011 \pm 0.000\,013$ d. The planet equilibrium temperature ($T_{\mathrm{equ}} = 1500$ K) and the bright host star ($V = 10.4$ mag) make it a good candidate for follow-up atmospheric studies.

Key words: methods: data analysis – methods: observational – techniques: photometric – stars: individual: WASP-13 – planetary systems.

1 INTRODUCTION

The discovery of the first short-period transiting planet HD 209458b (Charbonneau et al. 2000; Henry et al. 2000) opened a new field of exoplanetary research. Their advantageous geometry allows us to estimate accurate planetary mass and radii. The bulk density of the planet provides information on its composition (Guillot 2005; Fortney, Marley & Barnes 2007) and places constraints on planetary structure and formation models.

Interestingly, many of the short-period planets are bloated relative to baseline models (e.g. Bodenheimer, Laughlin & Lin 2003; Fortney et al. 2007), which assume a hydrogen/helium planet contracting under strong stellar irradiation. We define the radius anomaly of exoplanets as the difference between the measured radius and theoretical radius. Negative radius anomalies, i.e. denser planets, can be explained by different planet composition or/and the presence of a core (Guillot et al. 2006; Burrows et al. 2007). However, the majority of the hot giant planets have low density (i.e. radius anomalies larger than zero) that are harder to reconcile. Several theories have been presented to explain the positive radius anomalies of hot exoplanets: these include tidal heating (Bodenheimer, Lin & Mardling 2001), kinetic heating due to winds (Guillot & Showman 2002), enhanced atmospheric opacities (Burrows et al. 2007) and Ohmic dissipation (Batygin, Stevenson & Bodenheimer 2011). Although these theories can explain individual systems, only the recent ohmic dissipation theory (Batygin et al. 2011) can successfully explain all of the known exoplanets' radius anomalies (Laughlin, Crismani & Adams 2011). The lowest density hot Jupiters, such as WASP-13b, are particularly important to shed light on the physical mechanisms that lead to inflated planets.

For bright transiting systems, further insight into their physical properties can be obtained through follow-up observations. Transmission spectroscopy, which consists of measuring the stellar light filtered through the planet's atmosphere during transit, provides information into exoplanet atmospheres (Charbonneau et al. 2002; Vidal-Madjar et al. 2003). Observation of secondary eclipses (i.e. occultations) offers the potential for directly measuring planetary emission spectra (e.g. Deming et al. 2005; Charbonneau et al. 2008; Grillmair et al. 2008). Finally, the ability to measure the

⋆E-mail: s.barros@qub.ac.uk

sky-projected angle between the stellar rotation axis and planetary orbit, through the Rossiter–McLaughlin effect (McLaughlin 1924; Rossiter 1924), can yield clues about the formation and migration processes (Fabrycky & Winn 2009; Triaud et al. 2010; Winn et al. 2010).

Follow-up opportunities benefit from accurate planetary and stellar parameters. However, obtaining high signal-to-noise ratio transit observations from the ground is difficult. Consequently, even some of the planets with bright host stars are lacking good-quality light curves, and hence have poorly determined planetary parameters. This is the case for WASP-13b (Skillen et al. 2009) where it was not possible to accurately constrain the impact parameter ($0 < b < 0.46$) due to the lack of a high-precision transit light curve.

WASP-13b is a low-mass planet with $M_{\rm p} = 0.46 \pm 0.06 M_{\rm Jup}$ in a 4.3-d circular orbit (Skillen et al. 2009). Its host star is G1V type with $M_* = 1.03 \pm 0.10\,{\rm M}_\odot$, $T_{\rm eff} = 5826 \pm 100$ K, $\log g = 4.04$ and solar metallicity. WASP-13b was discovered in 2006–07 by the SuperWASP-North survey (Pollacco et al. 2006). As mentioned above, the impact parameter is not well constrained, and two possible sets of system parameters are presented in the discovery paper for two possible impact parameters; $b = 0$ and 0.46. This results in large uncertainties in both stellar ($R_* \sim 1.2$–$1.34\,{\rm R}_\odot$) and planetary radii ($R_{\rm p} \sim 1.06$–1.21). The adopted solution $b = 0.46$ suggests that the host star has evolved off the main sequence to the hydrogen-shell-burning phase. Therefore, this system is interesting in the context of exoplanet evolution, and with a bright host star ($V = 10.4$ mag) is a good candidate for follow-up studies.

In this paper, we present four high-precision transit observations of WASP-13b which are described in Section 2. Our data allow us to determine the inclination of the system and directly derive the mean stellar density and hence better constraint the stellar and planetary radii. We discuss our transit model in Section 3 and present the updated parameters of the system in Section 4. In Section 5, we discuss the discrepancy between theoretical and empirical limb-darkening coefficients (LDCs). Finally, we discuss our results in Section 6.

2 OBSERVATIONS

WASP-13b was observed with RISE (Gibson et al. 2008; Steele et al. 2008; Barros et al. 2011) mounted on the 2.0-m Liverpool Telescope on La Palma, Canary Islands. RISE is a frame transfer e2v CCD with a pixel scale of 0.54 arcsec pixel^{-1} that results in a 9.4×9.4 arcmin field of view. It has a wideband filter covering ~500–700 nm which corresponds approximately to $V + R$. For exposures longer than 1 s, RISE has a dead time of only 35 ms. To reduce the dead time to the minimum (Barros et al. 2011), we used an exposure time of 1 s which required a defocusing of -1.0 mm to avoid saturation of the bright comparison star (8.7 mag). Defocusing is also important to decrease systematic noise due to poor guiding (Barros et al. 2011).

The data were reduced using the ULTRACAM pipeline (Dhillon et al. 2007) which is optimized for time series photometry. Each frame was bias subtracted and flat-field corrected. We performed differential photometry relative to an ensemble of comparison stars in the field, confirmed to be non-variable. For each observation, we sampled different aperture radii and chose the aperture radius that minimized the noise. The photometric errors include shot noise, readout and background noise.

On 2009 January 29, we obtained an ingress of WASP-13b and an egress on 2009 May 05. We obtained full transits of WASP-13b on 2010 February 03 and 2011 January 13. Unfortunately, both observations were degraded by some clouds. Observations with transparency lower than 94 per cent were clipped. On 2010 February 03, the transit observation was interrupted after ingress due to the derotator reaching its limiting position, and the two parts of this transit are treated as separate observations. This observation shows systematics near the rotator interruption and is affected by clouds before the egress. We experimented removing it from the final analysis and concluded that its inclusion does not bias the results. On the last 20 min of the 2011 January 13 observation, the position of the star in the CCD varied by 10 pixels in the x and 15 pixels in y which caused an additional trend in the light curve. Due to its effect on the normalization of the light curve, the last 20 min of the 2011 January 13 observation were clipped. The number of exposures taken, estimated full width at half-maximum (FWHM) and aperture radius used for each observation are given in Table 1. We also included in our analysis, the previously published transit of WASP-13 taken with 0.95-m James Gregory Telescope (JGT) at St Andrews University on 2008 February 16 (Skillen et al. 2009).

Table 1. WASP-13 observation log.

Date	Number exposures	FWHM (pixel)	Aperture radius (pixel)
2009 January 29	4400	17	23
2009 May 05	10 780	21	24
2010 February 03	17 000	17	22
2011 January 13	16 000	24	27

The final high-precision transit light curves for WASP-13b are shown in Fig. 1 along with the best-fitting model described in Section 3.2. We overplot the model residuals and the estimated uncertainties, which are discussed in Section 3.1. To illustrate the quality of our results, we also show the phase-folded weighted combination of all the light curves in Fig. 2. Around -0.01 in phase, the only high-precision data are from the 2011 January 13 light curve that shows extra scatter and is below the transit model. The remaining transit phases are better sampled and hence have smaller errors.

3 DATA ANALYSIS

3.1 Photometric errors

As mentioned above, the initial photometric errors include only shot noise, readout and background noises, which underestimate the true errors. To obtain a more reliable estimate of the errors, we begin by scaling the errors of each light curve so that the reduced χ^2 of the best-fitting model is 1.0. This resulted in the multiplication of the errors by 1.01, 1.55, 2.46, 2.68, 2.26 and 2.79, for the 2008, 2009 January, 2009 May, 2010 ingress, 2010 egress and 2011 light curves, respectively. For the RISE observations, this indicates that the photometric errors are higher than expected from photon noise, probably due to the non-photometric conditions of these observations.

Exoplanet transit observations are also affected by time-correlated noise which can lead to underestimated parameter uncertainties (Pont, Zucker & Queloz 2006; Carter & Winn 2009). The residuals displayed in Fig. 1 show that the photometric noise is dominated by white noise. Nevertheless, we included time-correlated noise following the procedure from Gillon et al. (2009). Using the residuals of the best-fitting model, we estimated the amplitude of the red noise, $\sigma_{\rm r}$, to be 100 ppm (2009 January), 50 ppm

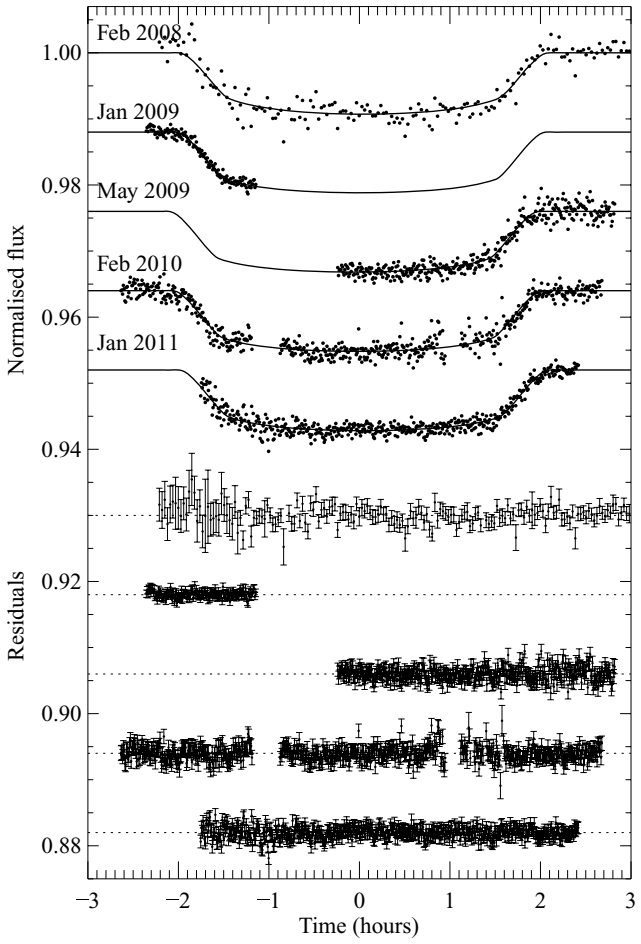

Figure 1. Transit observations of WASP-13b. From top to bottom in chronological order; JGT 2008 February 16, RISE 2009 January 01, RISE 2009 May 05, RISE 2010 February 03 and RISE 2011 January 13. We superimpose the best-fitting transit model and also show the residuals for each light curve at the bottom of the figure. The RISE data are binned into 30-s periods, and bins displaced vertically for clarity. The individual RISE light curves plotted here are available in electronic form at CDS and as Supporting Information with the online version of this article.

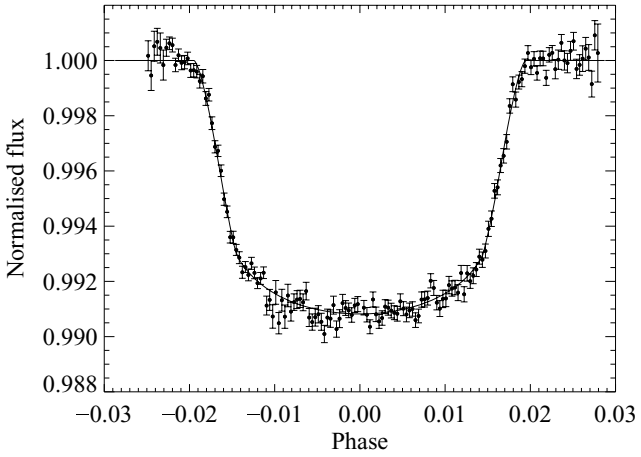

Figure 2. Phase-folded combined transit light curve of WASP-13b. The data were optimally binned in 150 phase bins for clarity. We superimpose the best-fitting transit model. Note that here we do not account for the different LD of the RISE and the JGT light curves.

(2009 May), 250 ppm (2010 ingress), 150 ppm (2010 egress) and 200 ppm (2011). For the 2008 light curve, the red noise was found to be negligible. These errors were added in quadrature to the rescaled photometric errors and were used in the final Markov chain Monte Carlo (MCMC) chains.

3.2 Determination of system parameters

To determine the planetary and orbital parameters, we fitted the four RISE light curves and the original JGT light curve of WASP-13b simultaneously. We used the same procedure as for WASP-21b (Barros et al. 2011) which is based on the Mandel & Agol (2002) transit model parametrized by the normalized separation of the planet, a/R_*, ratio of planet radius to star radius, R_p/R_*, orbital inclination, i, and the transit epoch, T_0, of each light curve. We account for a linear trend with time for each light curve parametrized by the out-of-transit flux and flux gradient. Due to the short orbital period and age of the system, we expect the orbit has circularized (see below), hence a circular orbit was assumed. The transit model is coupled with an MCMC procedure to obtain accurate parameters and uncertainties as outlined in Barros et al. (2011). We included the quadratic LDCs from the models of Howarth (2011a) for $T_{\rm eff} = 6000$ K, $\log g = 4.0$ and [M/H] = 0.0 which were the closest tabulations to the parameters from Skillen et al. (2009); for the RISE filter $V + R$, $a = 0.4402$ and $b = 0.2394$ and for the R filter of JGT, $a = 0.4121$ and $b = 0.2312$. We initially kept the LD parameters fixed during the fit. We treated the two parts of the 2010 February 03 observations as separate transits to correctly account for the normalization but restricted them to have the same T_0. Including the two linear normalization parameters for each light curve, a total of 20 parameters were fitted. Besides the linear normalization, no extra trends were removed from the light curves.

We computed seven MCMC chains, each of 500 000 points and different initial parameters. The initial 20 per cent of each chain that corresponded to the burn-in phase were discarded and the remaining parts merged into a master chain. We define the best-fitting parameter as the mode of its probability distribution and the 1σ limits as the value at which the integral of the distribution equals 34.1 per cent from each side of the mode. The Gelman & Rubin (1992) statistic was calculated for each fitted parameter, and we concluded that chain convergence was good.

To test how the LDCs affect the derived system parameters, we experimented with fitting the LDCs of the RISE light curves which have higher precision. Our tests indicate that the quality of the RISE light curves is not enough to fit for both LDCs (see also Gibson et al. 2008), and hence, we choose to fit the linear LDC a which dominates. The quadratic LDC of the RISE light curves b and both LDCs of the JGT light curve were kept fixed. Therefore, in this second MCMC procedure, 21 parameters were fitted.

4 RESULTS

In Table 2, we present the system parameters of WASP-13 and the 1σ uncertainties derived from the MCMC analysis for both the fixed and fitted LDCs. The first set of parameters can be directly derived from the light-curve analysis. The parameters were derived using the equations of Seager & Mallén-Ornelas (2003), Southworth, Wheatley & Sams (2007) and Kipping (2010). Specifically, the T_{1-4} refers to the total transit duration and T_{T1} is defined by equation (15) of Kipping (2010).

The derived linear LDC, $a = 0.34 \pm 0.03$, is statistically significantly different from the theoretical value $a = 0.4402$. The chain

Table 2. WASP-13 system parameters.

Parameter	LDC fixed	LDC fitted
Linear LDC for RISE a	0.4255	0.337 ± 0.033
Normalized separation a/R_*	$7.58^{+0.15}_{-0.13}$	$7.39^{+0.14}_{-0.15}$
Planet/star radius ratio R_p/R_*	$0.092\,253\,32^{+0.000\,80}_{-0.000\,81}$	$0.092\,26^{+0.000\,83}_{-0.0010}$
Transit duration T_{1-4} (h)	$4.094^{0.024}_{-0.033}$	$4.063^{0.026}_{-0.032}$
Transit duration T_{T1} (h)	$3.607^{0.012}_{-0.015}$	$3.548^{0.019}_{-0.017}$
Orbital inclination I (°)	85.64 ± 0.24	85.19 ± 0.26
Impact parameter b (R_*)	0.575 ± 0.020	0.621 ± 0.021
Stellar density ρ_* ($\rho_\odot$)	$0.309^{+0.018}_{-0.016}$	$0.288^{+0.019}_{-0.015}$
Orbital semimajor axis a (au)	$0.053\,79^{+0.000\,77}_{-0.000\,59}$	$0.053\,62^{+0.000\,74}_{-0.000\,85}$
Stellar mass M_* ($M_\odot$)	1.085 ± 0.04	1.09 ± 0.05
Stellar radius R_* ($R_\odot$)	$1.512^{+0.031}_{-0.041}$	1.559 ± 0.041
Planet mass M_p (M_{Jup})	$0.485^{+0.042}_{-0.058}$	$0.477^{+0.044}_{-0.049}$
Planet radius R_p (R_{Jup})	$1.365^{+0.034}_{-0.062}$	$1.389^{+0.045}_{-0.056}$
Planet density ρ_p (ρ_J)	$0.190^{+0.028}_{-0.014}$	$0.167^{+0.017}_{-0.022}$

convergence was good, and the linear LDC parameter is well constrained by our observations. We adopt the fitted LDC solution because according to the F-test, it is statistically significantly better (99.9 per cent) than the fixed LDC one. In Section 5, we present a more in-depth discussion about the discrepancy between the fitted and theoretical LDCs.

All the parameters of both solutions are within $\sim 3\sigma$. We found that the inclination of the orbit is $85\overset{\circ}{.}2 \pm 0\overset{\circ}{.}3$, and the derived stellar density is $0.29 \pm 0.02\,\rho_\odot$. This is significantly lower than previously assumed ($\rho_* = 0.43\,\rho_\odot$; Skillen et al. 2009), implying an evolved star. To obtain the stellar and planetary radii, we need to determine the stellar mass, as explained in the next section.

4.1 Stellar mass and age

Our high-quality transit light curves allow an accurate estimate of the stellar density. This, combined with stellar models, can be used to constrain the stellar mass and age. We interpolate the Yonsei–Yale evolution tracks (Demarque et al. 2004) for [Fe/H] = 0 (Skillen et al. 2009) which are plotted in Fig. 3. Also shown are the position of WASP-13 with the effective temperature from Skillen et al. (2009) and our value of ρ_*. We derive a stellar mass of $1.09 \pm 0.05\,M_\odot$ and a stellar age of 7.4 ± 0.4 Gyr. Both agree with the estimate in the original discovery paper. Using the stellar reflex velocity from Skillen et al. (2009), $K_1 = 55.7\,\mathrm{m\,s^{-1}}$, we estimate a planetary mass of $0.48\,M_{Jup}$.

In Fig. 4, we show the evolutionary tracks for a stellar mass of 1.0, 1.09 and $1.2\,M_\odot$ adapted from Demarque et al. (2004), and we overplot the position of WASP-13. These models suggest that WASP-13 has evolved to the hydrogen-shell-burning phase and is close to entering the subgiant branch. However, the uncertainty in the WASP-13 metallicity ([Fe/H] = 0 ± 0.2) affects the determination of its evolutionary status. According to the Demarque et al. (2004) models, if WASP-13 has a metallicity of +0.2, then it could have a mass of $1.2\,M_\odot$ which is above the critical mass for the stellar cores to become convective and where details on the treatment of convective overshooting become important. Due to the convective cores, the shape of the evolutionary tracks for higher mass stars is different, as is shown in Fig. 4. In this case, WASP-13 would probably still be in the contraction phase before the hydrogen-shell-burning phase starts.

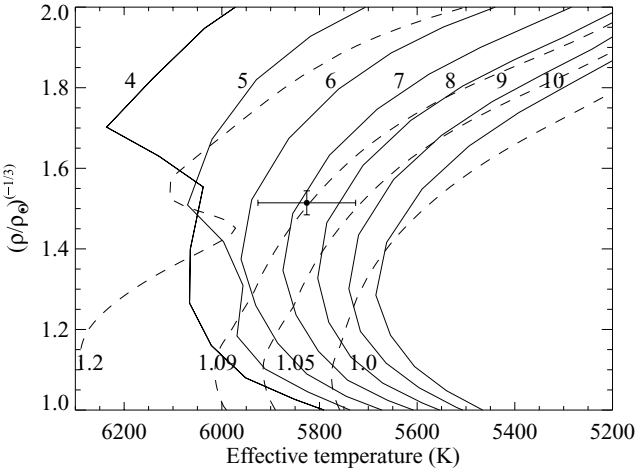

Figure 3. Isochrone models (solid lines) from Demarque et al. (2004) for WASP-13 using [Fe/H] = 0 from Skillen et al. (2009) and assuming solar composition $Z = 0.0181$. The age in Gyr is marked in the left of the respective model. We also show the mass tracks (dashed lines) for 1.0, 1.05, 1.09 and $1.2\,M_\odot$. We overplot the $T_{\rm eff} = 5826$ (Skillen et al. 2009) and our fitted $(\rho_*/\rho_\odot)^{-1/3}$ for WASP-13.

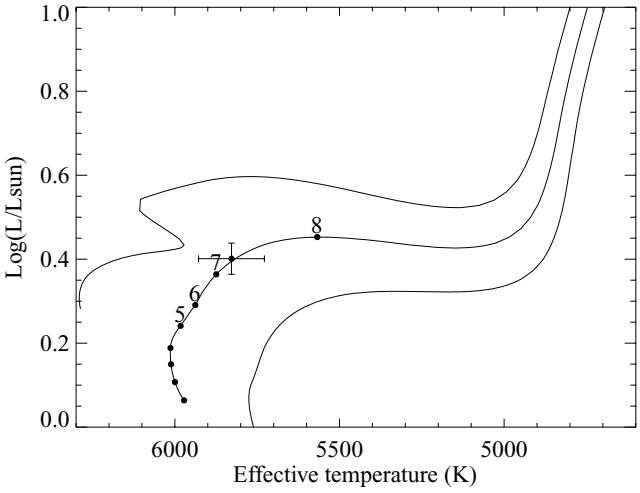

Figure 4. Evolutionary mass tracks from Demarque et al. (2004) for the same stellar parameters as Fig. 3 for stellar masses of 1.2, 1.09 and $1.0\,M_\odot$ from left to right. For the $1.09\,M_\odot$ evolutionary mass track, we also show the 5-, 6-, 7- and 8-Gyr points.

We obtain a larger stellar and planetary radius ($R_* = 1.56 \pm 0.04\,R_\odot$ and $R_p = 1.39 \pm 0.05 R_{Jup}$) than previously reported in Skillen et al. (2009). Our derived parameters are consistent with the '$b = 0.46$' adopted solution presented in the discovery paper, although our precision is almost 10 times better.

4.2 Transit times

The estimated transit times were used to update the linear ephemeris,

$$T(\mathrm{HJD}) = T_0 + \mathrm{EP}. \quad (1)$$

We found $P = 4.353\,011 \pm 0.000\,013$ d and $T_0 = 245\,5575.5136 \pm 0.0016$, which was set to the mid-transit time of the 2011 light curve. The updated period was used in the final MCMC procedures.

Time residuals from the linear ephemeris are given in Table 3. The partial transits show a larger deviation from the linear ephemeris

Table 3. Time residuals from the linear ephemeris.

Date	Epoch	Time residuals (s)	Uncertainty (s)
2008 February 16	−244	235	82
2009 January 29	−164	83	42
2009 May 05	−142	−211	51
2010 February 03	−79	−92	39
2011 January 13	0	114	44

which was also noted for the case of TrES-3b (Gibson et al. 2009). These authors concluded that the uncertainties in the transit times of partial transits are underestimated, probably due to the lack of out-of-transit data needed for normalization. Therefore, although the time residual of the 2009 May transit is significant at 4σ, this could be due to normalization errors rather than an intrinsic transit timing variation. For example, removing the out-of-transit data of the 2009 May light curve results in a difference in the estimated mid-transit time of 155 s $=3.5\sigma$. This suggests the presence of additional red noise in the light curve that affects the transit times which should be regarded with caution. Hence, we conclude that the time residuals of WASP-13b are probably consistent with a linear ephemeris, but encourage further transit timing observations.

5 LIMB DARKENING

Our measured linear LD parameter ($a = 0.34 \pm 0.03$) is statistically different from the one predicted from stellar models ($a = 0.4402$). We choose the theoretical LDCs from stellar models of Howarth (2011a) because they include the '$V + R$' RISE filter.

Disagreement between the empirical and theoretical LDCs has been reported for other systems (e.g. Southworth 2008; Barros et al. 2011) including for higher quality light curves from *Hubble Space Telescope* (*HST*; Claret 2009), *CoRoT* (Sing 2010; Csizmadia, in preparation) and *Kepler* (Kipping & Bakos 2011). This suggests that the discrepancy is not due to insufficient quality of our light curves. Moreover, Claret (2009) concluded that uncertainties in the stellar temperature and metallicity cannot explain the difference between the theoretical and empirical LDCs. Therefore, the causes of this discrepancy are not clear.

Recently, Howarth (2011b) showed that LDCs derived from transit observations depend on the impact parameter and cannot be directly compared with the theoretical values. This is because for a higher impact parameter, the transit shape is less sensitive to the global LD law. This can lead to up to a 60 per cent difference in the estimated LDCs (Howarth 2011b). Fortunately, this insensitivity also means that the effect on the transit parameters is relatively small. Using a synthetic photometry/atmosphere model, Howarth (2011b) predicts that this geometric effect leads to an underestimation of the linear LDC of the quadratic law which qualitatively explains our estimated linear LDC. If this was the only cause of the discrepancy, we should adopt the theoretical LDC solution for the system parameters because it would remove the correlation between the LDCs and the impact parameter providing more accurate results.

Using *HST* and *Kepler* data, Howarth (2011b) concluded that accounting for this geometrical dependency leads to better agreement between the measured and predicted LDCs. However, this cannot reproduce all of the empirical data, suggesting that there could be other causes of the discrepancy. Tentative explanations include the missing physics in the atmospheric models like, for example, the effects of faculae and granulation (Csizmadia et al., in preparation) and the plane-parallel approximation in stellar models (Neilson & Lester 2011). In this case, it would be advisable to adopt the fitted LDC solution for the system parameters because it is less dependent on the stellar models.

Further investigation of very high precision transit light curves such as from the *Kepler* mission is needed to better understand the difference between the measured and theoretical LDCs. This will help to decide if we should fit for the LDCs in lower quality light curves.

6 DISCUSSION AND CONCLUSION

We have presented four new transit light curves of WASP-13b including two full transits. To derive the parameters of the system, we used the same MCMC procedure as Barros et al. (2011) by fitting these new light curves together with a previous JGT transit of WASP-13b (Skillen et al. 2009). We estimated the uncertainties accounting for formal errors and systematic noise.

Our derived value of the linear LDC is statistically significantly different from the theoretical value predicted by stellar atmosphere models. Although this does not significantly affect the derived system parameters, it can be important for stellar atmosphere models. We adopt the fitted LDC solution because it is a statistical significantly better fit to the data.

The impact parameter of WASP-13b was poorly constrained in the discovery paper ($0 < b < 0.46$) though the higher value was adopted. We obtain $b = 0.62 \pm 0.02$, which is close to the previous adopted value although slightly higher. This implies a larger stellar radius of $R_* = 1.56 \pm 0.04\,\mathrm{R}_\odot$ which combined with the evolution models of Demarque et al. (2004) points to an age of 7.4 ± 0.4 Gyr for the host star. It also suggests that WASP-13 has evolved off the main sequence and is now in the hydrogen-shell-burning phase which would imply that in less than 2 Gyr the star will engulf the planet's current orbit. The evolutionary status of WASP-13 favours a slightly higher mass for the host star of $\sim 1.1\,\mathrm{M}_\odot$ which also implies a slightly higher planetary mass of $0.48 M_{\mathrm{Jup}}$.

We derived a larger planetary radius for WASP-13b, ($R_\mathrm{p} = 1.39 \pm 0.05 R_{\mathrm{Jup}}$), than previously reported and hence a lower density, ($\rho_\mathrm{p} = 0.17 \pm 0.01 \rho_\mathrm{J}$). Therefore, WASP-13b is the fifth lowest density exoplanet known after Kepler-7b (Latham et al. 2010), WASP-17b (Anderson et al. 2010), TrES-4b (Mandushev et al. 2007) and CoRoT-5b (Rauer et al. 2009), and its properties are important for irradiation models. We estimate an equilibrium temperature for WASP-13b of $\sim$1500 K. The hydrogen/helium coreless models of Fortney et al. (2007) predict a radius of $\sim 1.1 R_{\mathrm{Jup}}$ for WASP-13b. This is in agreement with the radius derived from the polynomial fit of Laughlin et al. (2011) to the baseline models of Bodenheimer et al. (2003), $R_\mathrm{p} \sim 1.16$. We derive a radius anomaly for WASP-13b of $\Re = 0.23$ (Laughlin et al. 2011). Therefore, WASP-13b is inflated relative to the theoretical thermal irradiation models for gas giant planets.

The circularization time-scale for WASP-13b is 0.011–0.11 Gyr for $Q_\mathrm{p} = 10^5$–10^6. Therefore, we expect a circular orbit, and it is unlikely that the inflated radius of WASP-13 could be explained by tidal dissipation. Enhanced atmospheric opacities of 10 times the solar, plus the correction due to the transit radius effect (Burrows et al. 2007), can explain a radius anomaly of $\sim$0.18 for a 7.4-Gyr planet and hence might be able to explain the radius anomaly of WASP-13b. The models of Bodenheimer et al. (2003) which include kinetic heating (Guillot & Showman 2002) can also explain the radius of WASP-13b. Finally, the Ohmic dissipation model of Batygin et al. (2011) explains all known exoplanet radii.

According to the classification of Fortney et al. (2008), WASP-13b belongs to the highly irradiated 'pM' class planets. These have considerable opacities due to molecular hazes of TiO and VO, and are expected to have temperature inversions in their atmosphere. This can be tested by secondary eclipse observations. The large-scale height of WASP-13b, ∼550 Km, and its bright host star, $V = 10.4$, makes it also a good target for transmission spectroscopy. Probing the atmospheric composition of this planet can shed light on its inflated radius.

ACKNOWLEDGMENTS

The RISE instrument mounted at the Liverpool Telescope was designed and built with resources made available from Queen's University Belfast, Liverpool John Moores University and the University of Manchester. The Liverpool Telescope is operated on the island of La Palma by Liverpool John Moores University in the Spanish Observatorio del Roque de los Muchachos of the Instituto de Astrofisica de Canarias with financial support from the UK Science and Technology Facilities Council. We thank Tom Marsh for the use of the ULTRACAM pipeline. SCCB is grateful to Yilen Gomez Maqueo Chew for useful comments. We also thank the anonymous referee for interesting suggestions.

REFERENCES

Anderson D. R. et al., 2010, ApJ, 709, 159
Barros S. C. C., Pollacco D. L., Gibson N. P., Howarth I. D., Keenan F. P., Simpson E. K., Skillen I., Steele I. A., 2011, MNRAS, 416, 2593
Batygin K., Stevenson D. J., Bodenheimer P. H., 2011, ApJ, 738, 1
Bodenheimer P., Lin D. N. C., Mardling R. A., 2001, ApJ, 548, 466
Bodenheimer P., Laughlin G., Lin D. N. C., 2003, ApJ, 592, 555
Burrows A., Hubeny I., Budaj J., Hubbard W. B., 2007, ApJ, 661, 502
Carter J. A., Winn J. N., 2009, ApJ, 704, 51
Charbonneau D., Brown T. M., Latham D. W., Mayor M., 2000, ApJ, 529, L45
Charbonneau D., Brown T. M., Noyes R. W., Gilliland R. L., 2002, ApJ, 568, 377
Charbonneau D., Knutson H. A., Barman T., Allen L. E., Mayor M., Megeath S. T., Queloz D., Udry S., 2008, ApJ, 686, 1341
Claret A., 2009, A&A, 506, 1335
Demarque P., Woo J., Kim Y., Yi S. K., 2004, ApJS, 155, 667
Deming D., Seager S., Richardson L. J., Harrington J., 2005, Nat, 434, 740
Dhillon V. S. et al., 2007, MNRAS, 378, 825
Fabrycky D. C., Winn J. N., 2009, ApJ, 696, 1230
Fortney J. J., Marley M. S., Barnes J. W., 2007, ApJ, 659, 1661
Fortney J. J., Lodders K., Marley M. S., Freedman R. S., 2008, ApJ, 678, 1419
Gelman A., Rubin D., 1992, Statistical Sci., 7, 457
Gibson N. P. et al., 2008, A&A, 492, 603
Gibson N. P. et al., 2009, ApJ, 700, 1078
Gillon M. et al., 2009, A&A, 496, 259
Grillmair C. J. et al., 2008, Nat, 456, 767
Guillot T., 2005, Annu. Rev. Earth Planet. Sci., 33, 493
Guillot T., Showman A. P., 2002, A&A, 385, 156
Guillot T., Santos N. C., Pont F., Iro N., Melo C., Ribas I., 2006, A&A, 453, L21
Henry G. W., Marcy G. W., Butler R. P., Vogt S. S., 2000, ApJ, 529, L41
Howarth I. D., 2011a, MNRAS, 413, 1515
Howarth I. D., 2011b, MNRAS, doi:10.1111/j.1365-2966.2011.19568.x
Kipping D. M., 2010, MNRAS, 407, 301
Kipping D., Bakos G., 2011, ApJ, 730, 50
Latham D. W. et al., 2010, ApJ, 713, L140
Laughlin G., Crismani M., Adams F. C., 2011, ApJ, 729, L7
McLaughlin D. B., 1924, ApJ, 60, 22
Mandel K., Agol E., 2002, ApJ, 580, L171
Mandushev G. et al., 2007, ApJ, 667, L195
Neilson H. R., Lester J. B., 2011, A&A, 530, A65
Pollacco D. L. et al., 2006, PASP, 118, 1407
Pont F., Zucker S., Queloz D., 2006, MNRAS, 373, 231
Rauer H. et al., 2009, A&A, 506, 281
Rossiter R. A., 1924, ApJ, 60, 15
Seager S., Mallén-Ornelas G., 2003, ApJ, 585, 1038
Sing D. K., 2010, A&A, 510, A21
Skillen I. et al., 2009, A&A, 502, 391
Southworth J., 2008, MNRAS, 386, 1644
Southworth J., Wheatley P. J., Sams G., 2007, MNRAS, 379, L11
Steele I. A., Bates S. D., Gibson N., Keenan F., Meaburn J., Mottram C. J., Pollacco D., Todd I., 2008, in McLean I. S., Casali M., eds, Proc. SPIE Conf. Ser. Vol. 7014, RISE: A Fast-readout Imager for Exoplanet Transit Timing. SPIE, Bellingham, p. 70146J
Triaud A. H. M. J. et al., 2010, A&A, 524, A25
Vidal-Madjar A., Lecavelier des Etangs A., Désert J., Ballester G. E., Ferlet R., Hébrard G., Mayor M., 2003, Nat, 422, 143
Winn J. N., Fabrycky D., Albrecht S., Johnson J. A., 2010, ApJ, 718, L145

SUPPORTING INFORMATION

Additional Supporting Information may be found in the online version of this article:

Figure 1 data. The data for the individual RISE light curves plotted in Fig. 1.

Please note: Wiley-Blackwell are not responsible for the content or functionality of any supporting materials supplied by the authors. Any queries (other than missing material) should be directed to the corresponding author for the article.

This paper has been typeset from a TEX/LATEX file prepared by the author.